Biophysical Journal Volume 76 April 1999 1856–1867

Calcium Dynamics in the Extracellular Space of Mammalian Neural Tissue

David M. Egelman and P. Read Montague
Division of Neuroscience, Center for Theoretical Neuroscience, Baylor College of Medicine, Houston, Texas 77030 USA

ABSTRACT In the brain, hundreds of intracellular processes are known to depend on calcium influx; hence any substantial fluctuation in external calcium ($[Ca^{2+}]_o$) is likely to engender important functional effects. Employing the known scales and parameters of mammalian neural tissue, we introduce and justify a computational approach to the hypothesis that large changes in local $[Ca^{2+}]_o$ will be part of normal neural activity. Using this model, we show that the geometry of the extracellular space in combination with the rapid movement of calcium through ionic channels can cause large external calcium fluctuations, up to 100% depletion in many cases. The exact magnitude of a calcium fluctuation will depend on 1) the size of the consumption zone, 2) the local diffusion coefficient of calcium, and 3) the geometrical arrangement of the consuming elements. Once we have shown that using biologically relevant parameters leads to calcium changes, we focus on the signaling capacity of such concentration fluctuations. Given the sensitivity of neurotransmitter release to $[Ca^{2+}]_o$, the exact position and timing of neural activity will delimit the terminals that are able to release neurotransmitter. Our results indicate that mammalian neural tissue is engineered to generate significant changes in external calcium concentrations during normal activity. This design suggests that such changes play a role in neural information processing.

INTRODUCTION

Over a century ago, the Reticular Theory of the brain—which supposed nervous tissue to be a continuous network like the vascular system—was ousted by new evidence that neural tissue is an intricate network of *discrete* cells. This insight ushered in an important new question: How do cells communicate across the small spaces that separate them? Since the 1920s, neurotransmission has been the object of an enormous amount of investigation, leading to the modern idea that synaptic connections are sites of localized information transfer between pre- and postsynaptic neurons (Loewi and Navratil, 1926). There is an important element left out of this picture: discrete signaling elements like neurons and synapses are crowded tightly in neural tissue. This crowding sets up conditions under which certain extracellular ion concentrations may be limited in supply on short spatial and temporal scales (Nicholson et al., 1978; Heinemann et al., 1990; Smith, 1992; Montague, 1996). We concentrate here on external calcium ($[Ca^{2+}]_o$), given the widespread importance of calcium signaling, both externally and internally. For example, release of neurotransmitter displays a high sensitivity to $[Ca^{2+}]_o$ (Dodge and Rahamimoff, 1967; Katz and Miledi, 1970; Mintz et al., 1995; Qian et al., 1997). A short list of other processes affected by internal calcium changes includes production of messenger substances, gene regulation, plasticity, cytoskeletal shaping, ion-channel modulation, the balance of kinase and phosphatase activity, and general enzymatic activation (for a review, see Bootman and Berridge, 1995). We first employ known parameters of mammalian neural tissue to detemine whether large changes in calcium can be expected to occur; we then examine how the calcium changes may be read as signals and the end to which the signals may be employed.

We show below that, in the mammalian nervous system, a number of features combine to encourage large fluctuations in external calcium levels during normal neural activity. These include the concentration gradient for calcium (outside to inside), the amount of calcium consumed during an action potential, the geometry of the extracellular space (ECS), and the slowness of calcium pumps that put calcium back into the ECS. Taken together, these features of neural tissue ensure that 1) calcium movement through ionic channels is unidirectional, 2) diffusion is the primary mechanism of calcium replenishment on short time scales, and 3) diffusion in the interstices of the extracellular space is impeded relative to free diffusion.

In the mammalian brain, external calcium concentrations range from 1.5 to 2.0 mM (Jones and Keep, 1987), and intracellular levels ($[Ca^{2+}]_i$) range from 50 to 100 nM, yielding an outside-to-inside chemical gradient of 15,000–40,000:1. Combined with an electrical gradient (also pointing outside to inside at rest), an open calcium channel exposes calcium ions to an unusually large driving force. Thus open ionic pores through which there is a calcium flux provide a unidirectional path for rapid calcium movement out of the ECS. Replenishment of depleted $[Ca^{2+}]_o$ on rapid time scales occurs primarily through diffusion from nearby regions of the ECS (demonstrated below), because calcium extrusion by exchangers and pumps operates on time scales about two orders of magnitude slower than calcium influx and diffusion (Schatzmann, 1989; Philipson and Nicoll, 1993; Helmchen et al., 1996; Sinha et al., 1997).

Received for publication 16 April 1998 and in final form 25 January 1999.
Address reprint requests to Dr. P. Read Montague, Center for Theoretical Neuroscience, Division of Neuroscience, Baylor College of Medicine, 1 Baylor Plaza, Houston, TX 77030. Tel.: 713-798-3134; Fax: 713-798-3946; E-mail: read@bcm.tmc.edu.

0006-3495/99/04/1856/12 $2.00

Experimental techniques do not yet exist that permit rapid calcium measurements in the exquisitely small volumes of individual synaptic clefts, although ion-sensitive microelectrode studies, on a larger spatiotemporal scale, indicate that $[Ca^{2+}]_o$ can change substantially under normal conditions (Nicholson et al., 1978; Nicholson, 1980; Benninger et al., 1980; Sykova, 1997). Currently, analysis of small, rapid fluctuations is available only at the mathematical and simulation level. Analysis with partial differential equations is an unmanageable approach because of the complexity of the geometry of the ECS. Monte Carlo techniques are a traditional choice for simulating diffusion in complex geometries but incur too much computational cost for our purposes. Thus we have engineered a computational approach that allows us to capture, as simply and generally as possible, the character of $[Ca^{2+}]_o$ dynamics in the ECS.

MATERIALS AND METHODS

We have developed a finite-difference model of the extracellular space, programmed in C and run on Silicon Graphics workstations. In short, the model discretizes extracellular space into small units. Each unit interacts with its neighbors via local rules, and in this way accounts for calcium diffusion, depletion, and replenishment. Full details of the model and its comparison to Monte Carlo simulations can be found in Egelman and Montague (1998). A brief description follows here.

Simulating the tissue

We begin with a simulated tissue of cubic intracellular units (IUs) (Fig. 1 *A*). The side of each IU is set at 806 nm (Fig. 1 *B*), yielding the same volume as a sphere 1 μm in diameter. In this way, each IU is approximately sized to represent an axonal bouton or spinehead, and IUs can be linked together to simulate larger elements, such as dendrites and somas. The IUs are packed tightly together, with an ECS width on the order of 20 nm.

Diffusion

The ECS in the model is subdivided into small rectangles called *ECS units* (Fig. 1 *C*). Each ECS unit holds a single state variable $C(\tau)$, which represents the average calcium concentration in that volume at time step τ. At each time step, ECS units update $C(\tau)$ as a function of the concentrations of adjacent ECS units. It is straightforward to interpret the units as a discretized physical space, the variables as the local concentration of calcium atoms, and the evolution rules as diffusion of these atoms.

Consumption

The IUs, positioned on a simple cubic lattice, consume and extrude calcium. For consumption, an IU can be in either an active or an inactive state (active because of depolarization, ligand binding, intracellular cascades, etc.). In the active state, consumption takes place through some fraction of the surface of the IU, called the *consumption zone*. In the model, consumption is summed up in a single parameter, $P_c \epsilon [0,1]$. This parameter is engineered to correspond to Monte Carlo simulations: its value can be thought of as the probability that a random walking ion bumping into an active zone of the IU will be drawn in.

While P_c in a real neuron is a function of channel distribution and open probabilities, we approximate action potential invasion by adjusting P_c until an active zone consumes some desired number of ions over 1 ms (the width of an action potential). Usually this integrated current is set at 14,000 atoms/active zone/spike, following experimental evidence in the mammalian brain (Helmchen et al., 1997).

The discrete dynamics for consumption are derived from a simple statistical argument: of N randomly walking particles in an ECS unit, the fraction within striking distance of the cell surface in the next time step is given by the ratio of the step length along each axis, λ, to the total cleft height, Z. Of this fraction, half the atoms within reach will step toward the surface while the other half step away. Those that collide with the surface are absorbed with probability P_c, yielding

$$\Delta N = -\frac{1}{2}\frac{\lambda}{Z} N P_c \qquad (1)$$

The discretization of this equation yields a simple update rule for consumption at each time step.

Extrusion

In line with experimental and modeling data, calcium extrusion is taken as a first-order function of $[Ca^{2+}]_i$ (Tank et al., 1995). The extrusion rate is adjusted to yield a $[Ca^{2+}]_i$ half-life between $t^* = 35$ ms (Sinha et al., 1997) and several hundred milliseconds (Regehr and Tank, 1990; Tank et al., 1995; Helmchen et al., 1996). Because sequestered molecules are extruded

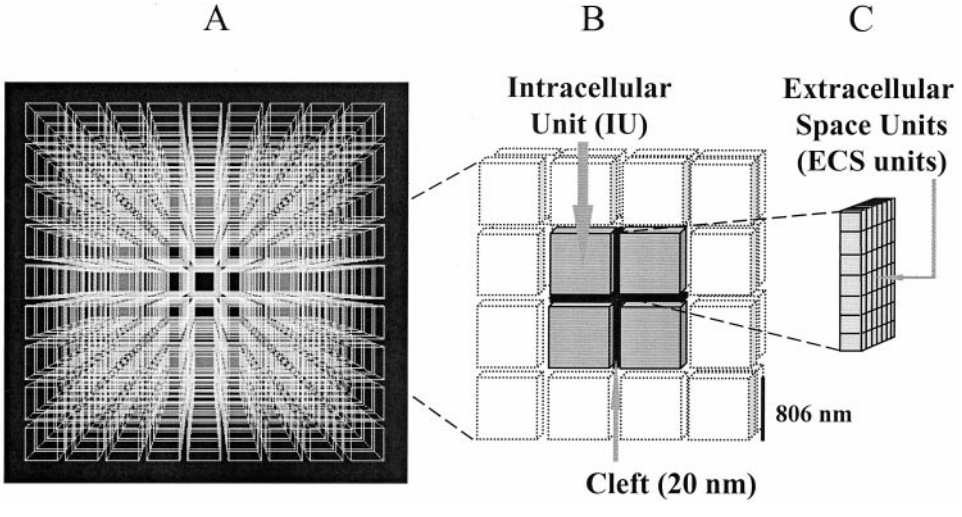

FIGURE 1 (*A*) Diagram of the three-dimensional discrete space model. (*B*) Elementary intracellular units (IUs) are cubes 0.806 μm on a side, which yields the same volume as a sphere 1.0 μm in diameter. (*C*) The clefts between the IUs are subdivided into smaller ECS units with side lengths of 115 nm (i.e., subdivisions of 7×7). Each ECS unit holds the average calcium concentration in that region. At each time step, each ECS unit updates its concentration as a function of the concentration of its contiguous neighbors and as a function of the activity of the intracellular units with which it is in contact. Time step is 2 μs, which simulates diffusion with very little error at the specified spatial scales (Egelman and Montague, 1998).

from their point of entry, this is equivalent to ignoring slow intracellular diffusion.

The model

The model can be thought of as interacting lattices, with the ECS units and intracellular units each holding sets of discrete variables, updated synchronously at each time step.

The concentration change in continuous form is described by

$$\frac{\partial C(x,t)}{\partial t} = D\frac{\partial^2 C(x,t)}{\partial x^2} - \text{sinks} + \text{sources} \qquad (2)$$

where the "sinks" term stands for the fast consumption through Ca^{2+}-fluxing channels, the "sources" term represents the slow replenishment by pumps and exchangers, and the three-dimensional vector character of **x** is left implicit.

We implement the dynamics discretely, using the following implementation for each ECS unit, *i*:

$$\Delta C_i = \text{fluxes} - \text{sinks} + \text{sources}$$

$$\Delta C_i = \frac{\tau}{\delta^2} D \sum_j (C_j - C_i) - \left[2 - \left(1 - \frac{\lambda}{2Z}P_c^1\right)^{\tau/\theta} + \left(1 - \frac{\lambda}{2Z}P_c^2\right)^{\tau/\theta}\right] C_i + (1 - e^{k\tau/t^*})[C_{int}^1 + C_{int}^2] \qquad (3)$$

The first term on the right side represents diffusion, where τ is the time step of the finite difference simulation (2 μs), δ is the distance between the centers of ECS units (115 nm), D is the local diffusion coefficient, and j sums over contiguous ECS neighbors. The second term represents depletion due to ion channels. Z is the cleft height (20 nm), and P_c^1 and P_c^2 are the consumption probabilities of the two IUs touching each ECS unit. $\lambda = \sqrt{2D\theta}$ is the average step length (along each Cartesian axis) of a randomly walking particle in time θ. A quick inspection of Eq. 3 will indicate that θ needs to be on the order of 50 ns, otherwise the step length of a particle will be close to or greater than the cleft height. In our simulations, $\tau \gg 50$ ns; therefore the second term is raised to the power of τ/θ, allowing us to account for the depletion that would take place in τ/θ instances of θ-size ticks. This issue is discussed in more detail in Egelman and Montague (1998).

The third term represents extrusion from intracellular compartments via pumps and exchangers: C_{int}^1 and C_{int}^2 are the intracellular calcium concentrations of the two IUs touching each ECS unit, t^* is the half-life, and $k = \ln(1/2)$.

Equation 3 represents a simple and straightforward way to represent the geometry in question. Setting up the computation in this manner is more feasible than a Monte Carlo approach, which is prohibitively time-intensive for large volumes of tissue.

Simulations use the following parameter values: τ (time step), 2 μs; δ (distance between ECS units), 115 nm; Z (cleft height), 20 nm; D (local diffusion coefficient), 300–600 $\mu m^2/s$; P_c (consumption parameter), 0.0–1.0. The values of τ and δ are carefully chosen to minimize error while counterbalancing computational expense (Egelman and Montague, 1998). The range of diffusion coefficients is justified in the next section (Fig. 3).

RESULTS

Diffusion coefficient and tortuosity in neural tissue

Calibration to neural tissue

The diffusion of calcium atoms in the networks of neural ECS will be slower than free diffusion, due at least to geometrical boundaries and buffering. The character and extent of extracellular calcium buffering are largely unknown, but presumably the effect of ECS buffers will be subsumed in the local diffusion coefficient. There are currently no measures of local diffusion coefficients, but the past two decades have given us several studies of long-distance diffusion parameters in the mammalian brain. Experiments were pioneered in the early 1980s in which a specific ion current was injected into one location in the brain, and the building concentration profile was measured at a distant site (30–200 μm away) (Nicholson, 1980; Nicholson and Phillips, 1981; Sykova, 1997). The results yield a dimensionless, empirical parameter called tortuosity, λ. Tortuosity relates the free diffusion coefficient, D_{free}, to the effective diffusion constant, D_{eff}:

$$D_{eff} = D_{free}/\lambda^2 \qquad (4)$$

Under nonpathologic conditions, λ lives within a narrow range of $1.5 \le \lambda \le 1.7$. This range encompasses measurements in different species, over different parts of the brain, and made with cations (calcium, tetramethylammonium, tetraethylammonium) or anions (α-naphthalene sulfonate and hexafluoroarsenate) (Nicholson, 1980; Nicholson and Phillips, 1981; Sykova, 1997). A value of $\lambda = 1.6$ reduces D from 600 $\mu m^2/s$ in free solution to 234 $\mu m^2/s$ in the brain.

Such studies do not specify the diffusion coefficient locally. Because tortuousity involves paths through the bulk geometry, such a measurement is mute on the speed with which a molecule can cross an individual synaptic cleft. To determine the value of λ inherent in our choice of geometry, we start 10,000 randomly walking atoms at a central point in a cubically packed volume of IUs and measure the RMS distance of the walkers as a function of time (Fig. 2 *A*). This allows us to use Eq. 4 to determine λ by the following:

$$r_{rms} = \sqrt{6D_{eff}t} \Rightarrow \lambda = \frac{\sqrt{6D_{free}t}}{r_{rms}} \qquad (5)$$

where the RMS distance of the walkers, r_{rms}, is measured as a function of t; D_{free} is set at 600 $\mu m^2/s$. The geometry of our simulated tissue yields $D_{eff} = 395$ $\mu m^2/s$, or $\lambda = 1.23$. Two possibilities, or a combination of the two, will account for the remaining slowing of diffusion measured in real tissue: 1) D_{local} is less than 600 $\mu m^2/s$, reflecting local extracellular binding, and/or 2) the extracellular space can be made more tortuous, as by the combination of elementary units into larger units (such as somas), or equivalently, some of the clefts can be clogged, acting as barriers to diffusion (Fig. 2 *B*). Because there is no way to cleanly balance these two possibilities, we will explore a wide parameter range, using $D_{local} = 300$ $\mu m^2/s$ and $D_{local} = 600$ $\mu m^2/s$ as lower and upper bounds.

It is important to note that the effect of restriction is not only the slowing of diffusion, but also the prolonged amplification of a signal. Fig. 2 *C* compares two cases: in the first, the tissue is cubically packed with IUs; in the second,

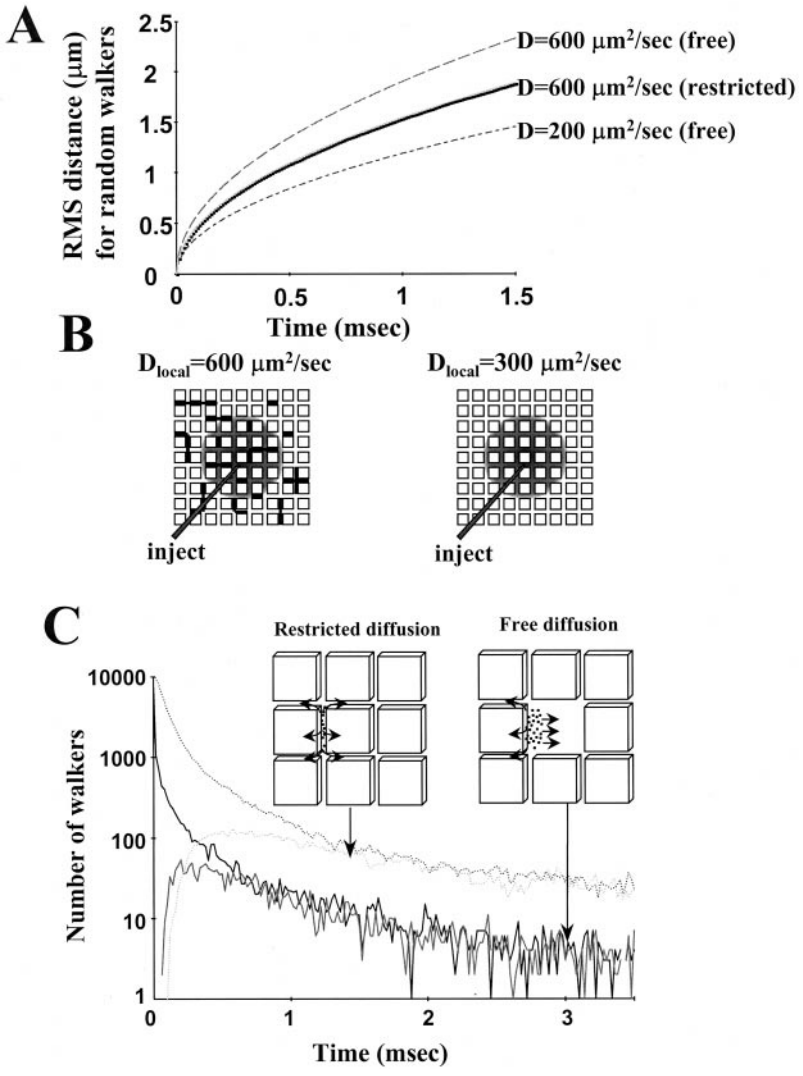

FIGURE 2 Diffusion within the extracellular space is slower than in free solution. In the nervous system, a single phenomenological parameter called *tortuosity* (λ) has been used to characterize the measured reduction in the free diffusion coefficient for movement in the ECS (e.g., see Nicholson and Phillips, 1981, or Sykova, 1997). Tortuosity is a stable number ($1.5 < \lambda < 1.7$) for calcium (Nicholson, 1980) and is the same for monovalent cations and anions (Sykova, 1997). (*A*) Root mean square distances for 10,000 random walkers versus time. The top trace ($D = 600\ \mu m^2/s$) and the bottom trace ($D = 200\ \mu m^2/s$) show results for unrestricted diffusion. The middle trace shows results in the presence of cubic intracellular units (IUs) for $D = 600\ \mu m^2/s$ ($9 \times 9 \times 9$ IUs). Introduction of these boundaries slows diffusion and approximates the free diffusion of a species with $D = 395\ \mu m^2/s$. (*B*) A combination of geometrical constraints and buffering serves to reduce the measured diffusion coefficient in the ECS. *Left*: Barriers in the ECS reduce the measured diffusion coefficient by slowing (on average) free diffusion. *Right*: Buffering by the extracellular matrix approximates a reduced diffusion coefficient throughout the ECS. (*C*) Restricted diffusion can structure a signal for a longer time. A signal carried by molecular diffusion in three dimensions (free diffusion) will quickly lose amplitude. If diffusion is restricted to a subspace (fewer degrees of freedom), as in the extracellular space of neural tissue, the concentration front can remain structured and resolvable for a longer time. The graph shows results of a Monte Carlo simulation: 10,000 atoms in the extracellular space walk randomly and reflect off the walls defined by the cubes (0.806 μm on a side). Two cases are examined: 1) the cube adjacent to the released walkers is present (restricted diffusion), and 2) the cube adjacent to the walkers is absent (free diffusion). The dotted lines show the number of walkers in the restricted diffusion case. The decaying trace is measured at the point where the walkers start, and the growing trace is measured at the other side of intervening cube. The solid lines show the number of walkers when there is no intervening cube. The measurements are made in the same volumes as in the restricted diffusion case. Note the logarithmic scale.

a cube is removed. As can be seen, with increasing free volume, the fluctuation diminishes more quickly.

Measurements of $[Ca^{2+}]_o$: effects of channel distribution

An important parameter in these simulations is the total number of Ca^{2+} atoms consumed during an action potential. In the mammalian central nervous system (CNS), Fura-2 overloading in the calyx of Held has allowed the measurement of the total calcium influx into the terminal during a single action potential invasion (Helmchen et al., 1997). Combined with an estimate of the total number of active zones, the total influx of calcium was estimated to be 14,000 atoms per active zone per spike. We begin with the assumption that each presynaptic unit in our model has only one

active zone, and we adjust the P_c to make our integrated current match the experimental data.

We will now demonstrate that the size of the calcium decrement will be a function not only of D_{local}, but also of the size of the active zone. A combination of structural and physiological methods indicates that calcium channels are concentrated at release zones (Smith and Augustine, 1988; Robitaille et al., 1990; Roberts et al., 1990; Qian et al., 1997). Therefore, knowing the desired integrated current, we look at the concentration decrement in a cleft caused by a total consumption of 14,000 Ca^{2+} atoms. When the calcium channels are spread evenly across the face of an intracellular unit (806 × 806 nm), local $[Ca^{2+}]_o$ can decrease by 10–20%, depending on the diffusion coefficient (Fig. 3 *A*). When the Ca^{2+} channels aggregate more tightly at an active zone, the local $[Ca^{2+}]_o$ can be almost completely depleted for the duration of an action potential (Fig. 3 *B*; active zone 115 × 115 nm).

Several Ca^{2+}-sensing mechanisms are likely to be expressed in the CNS, as considered in the Discussion. Examination of the surface plots in Fig. 3 shows that if calcium sensors are expressed in an area where calcium channels are spread widely (as in Fig. 3 *A*), the maximum Ca^{2+} decrement felt in the cleft may not be sufficient for detection. However, the clustering of calcium channels (Fig. 3 *B*) causes a large decrement to be felt throughout a substantial portion of the cleft.

As discussed above, we bound the local diffusion coefficient between $D = 300\ \mu m^2/s$ and $D = 600\ \mu m^2/s$. As can be seen in Fig. 3, *A* and *B*, higher diffusion coefficients prevent large decrements in the concentration, because the flow of calcium from neighboring extracellular space is rapid. Conversely, a lower D_{local} describes a more sluggish fluid, which allows a larger decrement to grow. For example, Fig. 3 *B* shows that when $D = 600\ \mu m^2/s$, the peak $[Ca^{2+}]_o$ decrement is 56%; for $D = 300\ \mu m^2/s$, the peak decrement reaches 91%.

Total consumption and diffusion limiting

Because different terminals in the CNS may consume more or less than 14,000 atoms per spike per active zone, we explore the parameter space by measuring the peak $[Ca^{2+}]_o$ decrement over a range of integrated currents (Fig. 4 *A*). The model predicts that the size of the calcium decrement is

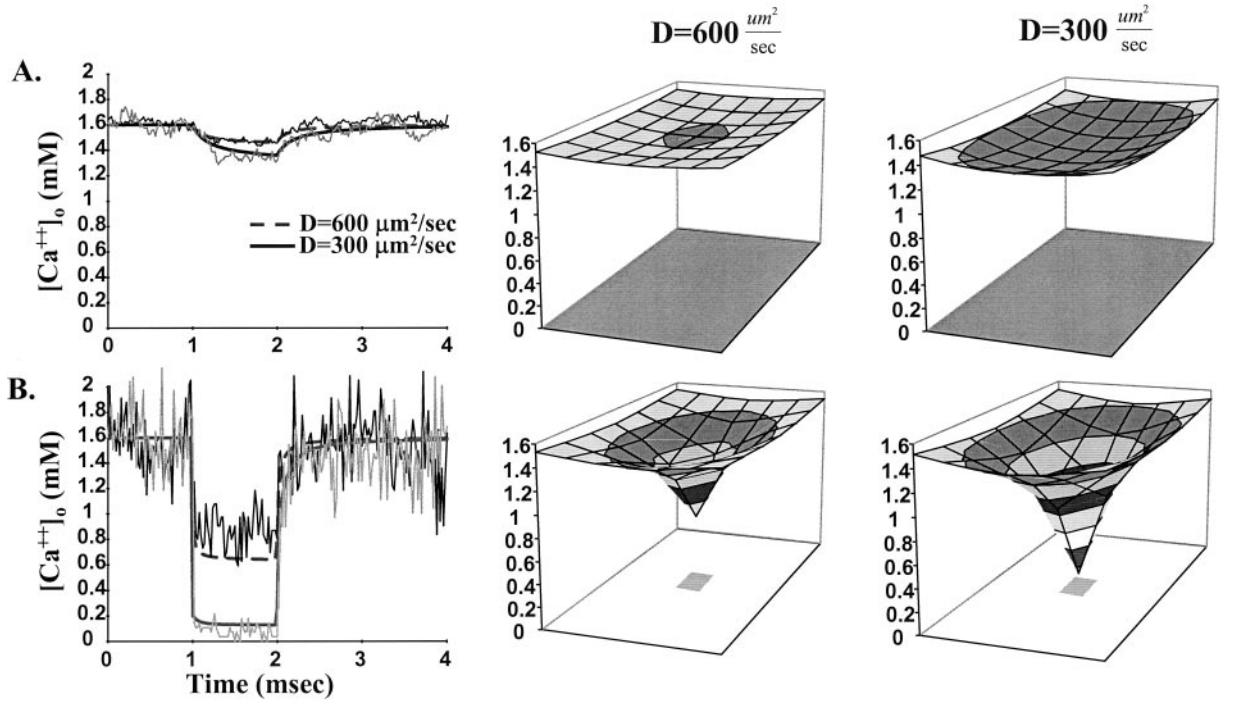

FIGURE 3 Calcium consumption through time: effects of changing active zone size and diffusion coefficient. At $t = 1$ ms, the calcium-fluxing active zone becomes active for 1 ms. The consumption parameter, P_c, is adjusted in each case for a total integrated consumption of 14,000 Ca^{2+} atoms (Helmchen et al., 1997). (*A*) Large active zone. Traces represent $[Ca^{2+}]_o$ available to the consuming zone; in this case, the calcium consumption is spread evenly over one face of an IU, making the consuming zone 806 × 806 nm. The dashed line shows the model results for $[Ca^{2+}]_o$ when the diffusion coefficient $D = 600\ \mu m^2/s$; for the solid line, $D = 300\ \mu m^2/s$. For comparison, jagged lines are results from Monte Carlo simulations; each trace reflects 6×10^5 walkers in a volume of 33.5 μm^3, with the same conditions and diffusion coefficients as the model. The panels to the right show snapshots of the concentration in the active cleft at $t = 2$ ms. (*B*) Small active zone. The size of the active zone is reduced to 115 × 115 nm, representing a clustering of the calcium conductances. The dashed line represents model results when $D = 600\ \mu m^2/s$; for the solid line, $D = 300\ \mu m^2/s$. Jagged lines are results from Monte Carlo simulations, again with 6×10^5 walkers, in the same conditions as the model. Because the area of measurement is smaller in this case (115 × 115 nm), the variance in the measurement is greater. For smaller active zones, there is a large local signal. If Ca-sensitive receptors are positioned near a tightly clustered active zone, they are more likely to sense a change in $[Ca^{2+}]_o$ than those in a spread-out zone.

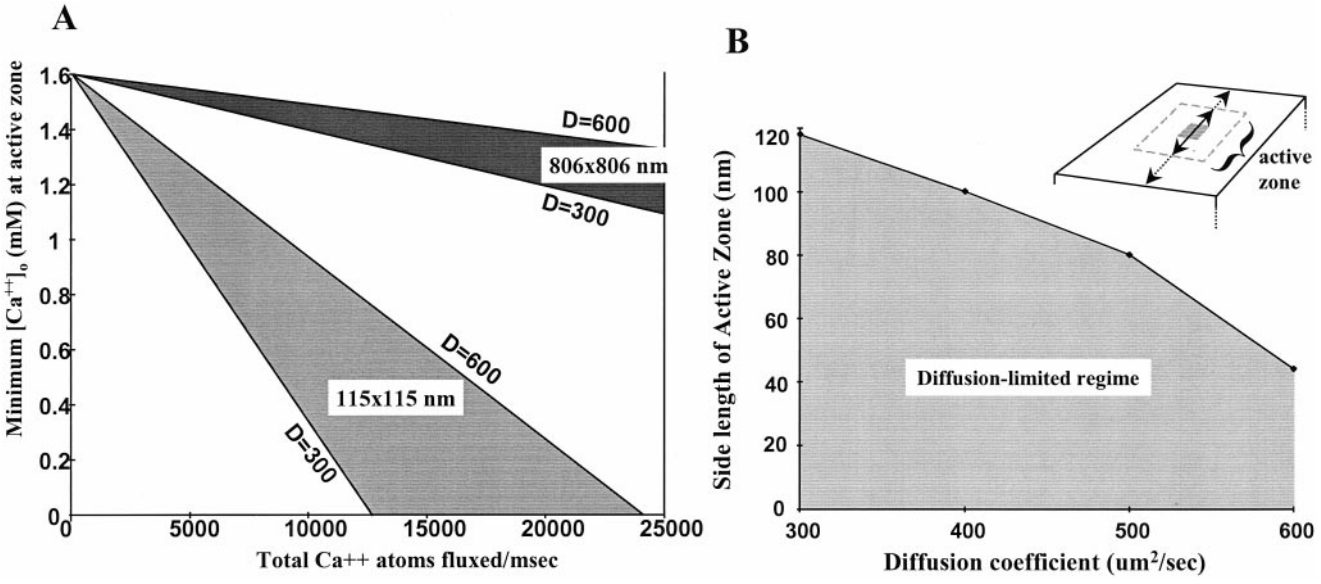

FIGURE 4 As an active zone grows smaller, an integrated consumption of 14,000 atoms may become impossible because of the slowness of diffusion. (*A*) Maximum $[Ca^{2+}]_o$ decrement in the active cleft plotted for different combinations of total Ca^{2+} current, local diffusion coefficients, and two different active-zone sizes. (*B*) Linear dimension of a square active zone plotted as a function of the local diffusion coefficient. The diffusion-limited region is shown in gray.

linearly related to the total consumption. As expected, the calcium decrement is sensitive to the diffusion coefficient and the size of the active zone as well. As can be seen in the figure, a dense packing of calcium channels can lead to total depletion of calcium within a large range of total influx estimates.

The clustering of calcium channels could become so tight that diffusion could not fill in rapidly enough to give an influx rate of 14,000 atoms/ms. In the example shown in Fig. 3 *B*, where the active zone is 115 × 115 nm and $D_{local} = 300\ \mu m^2/s$, only 12,000 atoms were consumed during a 1-ms period. Fig. 4 *B* shows that the active zone has to be a certain minimum size to consume 14,000 atoms; below that size, diffusion limits the total consumption.

Speed of recovery

Interestingly, although there is a large difference between the cases where the calcium channels are clustered and where they are not, the recovery to baseline concentration in the cleft follows a similarly rapid time course (Fig. 5). This indicates generally that one would not expect to see reduced calcium influx per spike from tetanic stimulation of anything less than 500 Hz, and indeed one does not (Atluri and Regehr, 1996). In other words, issues such as paired-pulse depression are not explained by a study of external calcium dynamics: when action potentials arrive >2 ms apart, $[Ca^{2+}]_o$ has had sufficient time to recover.

Cleft size as a control parameter

The degree to which the geometry slows extracellular diffusion will depend, in part, on the size of the clefts between cells. In this way, cleft size may be used as a control parameter to modulate signal strength. For the spatial scales of interest in the neural tissue, the cleft size is generally taken to be 20 nm. However, it is thought that cells (both glial and neuronal) may shrink or swell under various conditions (Sykova, 1997). Such shrinking or swelling results in complementary size changes in the ECS. It has been hypothesized that ECS size and geometry changes will affect the movement (diffusion) of various substances in the CNS (Nicholson, 1980; Nicholson and Phillips, 1981; Sykova, 1997). Here we examine the effect of cleft size changes on the signaling capacities of the extracellular fluid.

To that end, we activated one face of a single terminal in the middle of a volume of simulated tissue. The extracellular calcium signal in the overlying cleft was measured, and the cleft width was changed from 10 to 50 nm. As seen in Fig. 6, changing the cleft from 50 to 10 nm magnifies the signal strength by ~3.5-fold (from 7% to 25%). Our result that changes in cleft size modulate extracellular signaling is consonant with results from an analysis by Smith (1992) and discussions of pathologic changes in cleft size (Nicholson, 1980; Sykova, 1997). We assert that the dilation of blood vessels in a local region may compress the ECS of the cells between them. In that way, vasodilatation may serve a function in addition to oxygenation: blood flow may be the signal that sharpens calcium signaling in a region of tissue.

Is synaptic size significant?

Axonal terminals are large compared to the fine processes from which they blossom. Remarkably, the sizes of cortical synapses are conserved across species: even while the sizes of cell bodies and the length of processes vary, the volume of synaptic elements seems to remain constant (around 0.52

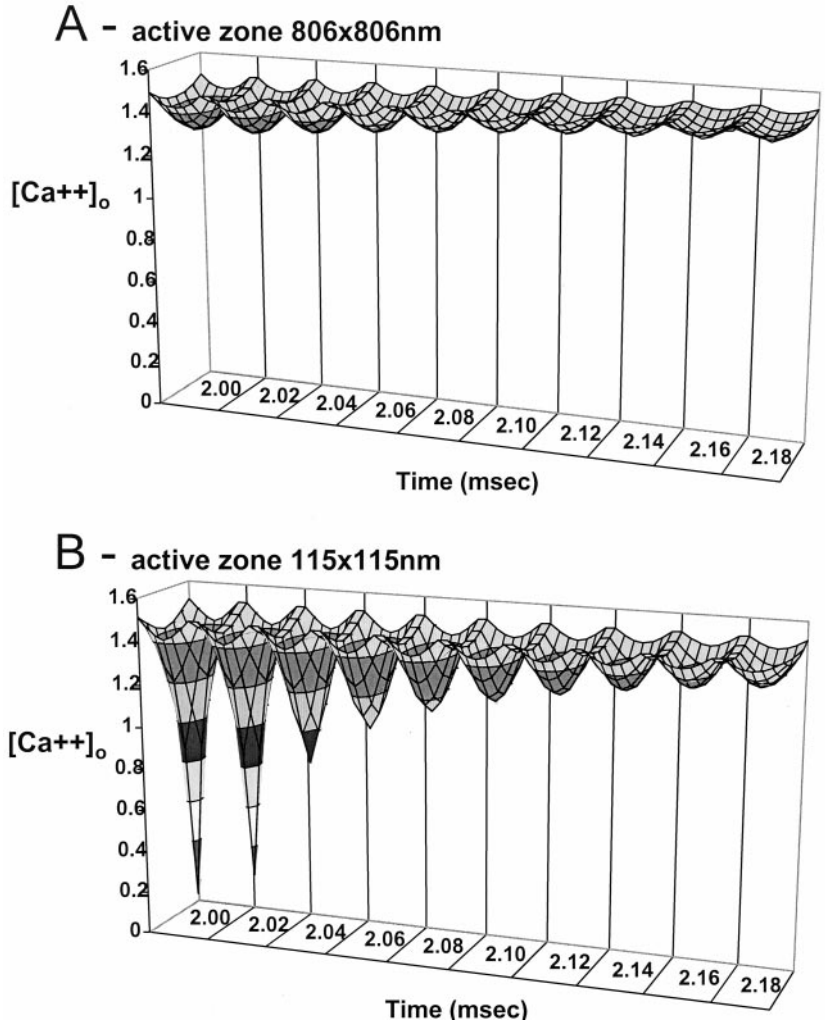

FIGURE 5 Active zone size has little effect on the recovery time of $[Ca^{2+}]_o$ after an action potential. Even for different sizes of active zones, the recovery time to baseline after an AP is approximately the same. Whatever the size of active zone, passive calcium dynamics will only play a part in paired-pulse effects if the separation is less than ~2 ms.

μm^3, or 1 μm in diameter). Here we attempt to determine whether there is anything special about this volume in light of extracellular calcium dynamics.

To examine the effects of changing the size of terminals, we shrunk the model intracellular units (IUs) from their default side length (806 nm) to 590 or 354 nm on a side, or expanded the unit to over double its side length at 1770 nm. As diagrammed in Fig. 7 *A*, the consuming zone always remained the same size at 115 × 115 nm. In all cases, the cleft size between the IUs was maintained at 20 nm. The consumption parameter, P_c, was adjusted for maximum consumption during a 1-ms action potential (total consumption in the default case is only 12,000, not 14,000 ions, because of diffusion limiting).

Fig. 7 *B* shows that the external calcium available to the active zone seems to be approximately the same, even for IUs of different sizes. Only the recovery times differ: when elements are larger, a longer time is required for the decrement to be filled back in.

In Fig. 7 *C* we measured the amplitude of the calcium decrement felt by a neighboring synaptic element—in this case, the neighbor on the opposite side of the IU (away from the active zone). As the IUs grow smaller, the signal felt one unit away from the active zone grows larger. In light of this, is there anything that appears to be special about the extant size of synaptic elements?

Standard statistical methods predict the expected density fluctuations in a volume of particles to be $\sigma = \sqrt{N}$. Thus, in a typically sized synaptic cleft (taken here to be 806 × 806 × 20 nm) at 1.6 mM resting concentration, we expect at any time to find 12,561 atoms plus or minus a standard deviation of 112 atoms. This is approximately a 1% fluctuation, which for a 1.6 mM resting concentration translates to a first standard deviation at 1.585 mM. It is interesting to note in Fig. 7 *C* that when an active zone on a $(806\ nm)^3$ terminal consumes, the peak fluctuation measured at the opposite side is almost exactly at 1.585 mM. In other words, the synapse may be appropriately sized to act as an autonomous unit, that is, consumption on one side of the unit should not exceed expected noise levels on the other side. When the units are made smaller (*lower two traces* in Fig. 7 *C*), then consumption on one side interferes with available calcium just one unit away.

It is important to keep in mind that we have clamped the total consumption to 12,000 atoms (in 1 ms) in the above examples. From the above results, we offer the following

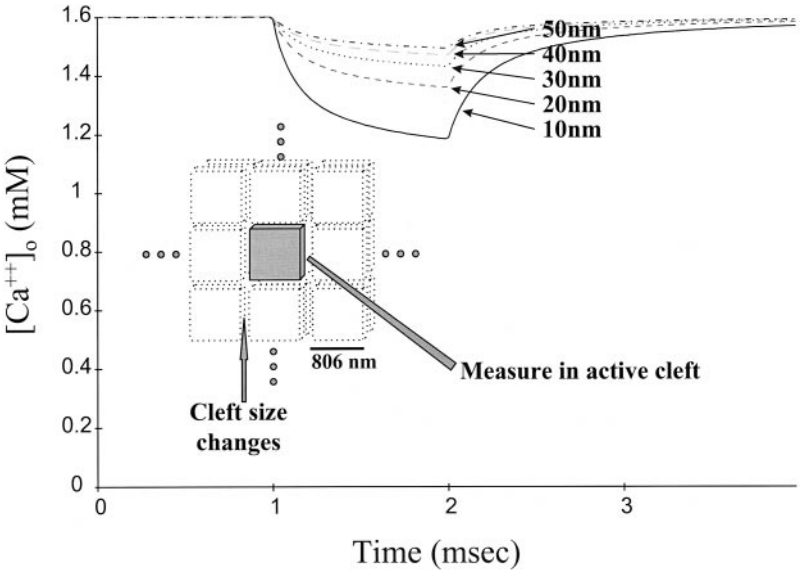

FIGURE 6 Cleft size as a control parameter. In the finite difference model, the consumption probability at a single presynaptic terminal is adjusted to consume 14,000 atoms in 1 ms across a single active face. By changing nothing but the cleft size, the extracellular signal is significantly modulated. In this example, $D = 600\ \mu m^2/s$.

speculation: if we assume that autonomy is the goal of the system (at least under normal circumstances), then a relationship is suggested between the signaling machinery (how many calcium atoms are consumed) and the volume of an element. We assume that synapses would prefer to be as small as possible (no wasted volume), but will grow to a size sufficient to make them autonomous units.

Signal propagation and terminal clustering

Although it is clear that large fluctuations may be expected at a terminal, it remains to be shown how far such a fluctuation will propagate. Fig. 8 *A* shows concentrations in contiguous clefts at different distances from a consuming presynaptic unit. It is seen that even for a large decrement, the signal attenuates quickly with distance. The calcium decrement that reaches neighboring clefts is approximately the same regardless of the size of the active zone (data not shown).

Thus far our discussion has been limited to single terminals. We now expand our view to examine what happens when terminals are clustered. An important motif in the nervous system is that not just one, but multiple boutons from a single axon will terminate in a region (Colman and Lichtman, 1992). Such arborization engenders synchronous calcium consumption (Mackensie et al., 1996) over a small region. Synchronous consumption may also arise from the correlation of different axons converging in the same region (see Discussion). Fig. 8 *B* demonstrates that even at distances where the fluctuation has decreased greatly from its original amplitude, synchronous activity may have noticeable effects on the resultant signal.

Background levels

The resting level of Ca^{2+} in the brain is not likely to ever be "at rest." To understand the effect of normal background activity on the baseline $[Ca^{2+}]_o$, we modeled a volume packed with randomly active units (Poisson firing rates; Fig. 8 *C*). Without extrusion mechanisms, the average cleft concentration drops to zero in 500 ms. However, with the addition of a biologically reasonable first-order extrusion mechanism, the background levels quickly reach a steady state. It is seen that higher activity in the region sets the baseline calcium concentration at lower levels.

As mentioned above, calcium extrusion via exchangers and pumps operates on a time scale approximately two orders of magnitude slower than the rapid calcium transient explored in this study (Schatzmann, 1989; Philipson and Nicoll, 1993; Helmchen et al., 1996; Sinha et al., 1997). As a result of the imbalance between the depletion and extrusion times, regional background activity may regulate the baseline Ca^{2+} concentration; such a level may set important parameters in attention, learning, or plasticity.

DISCUSSION

We have shown that $[Ca^{2+}]_o$ is expected to fluctuate during normal neural function. In the same way that a positive fluctuation in neurotransmitter concentration carries information by diffusing through the ECS, a negative fluctuation in an extracellular ion concentration will carry information as long as there are detecting elements. In the case of calcium, hundreds of intracellular processes (and perhaps some extracellular processes as well) are highly sensitive to calcium levels (Bootman and Berridge, 1995). Our results demonstrate that $[Ca^{2+}]_o$ is expected to change dynamically. Thus, not only synaptic connections—but also their relative positions and timing of activity—become important in understanding the function of the tissue.

Calcium fluctuations as a form of presynaptic inhibition

There is an obligatory relationship between calcium influx and neurotransmitter release: the dependence is approxi-

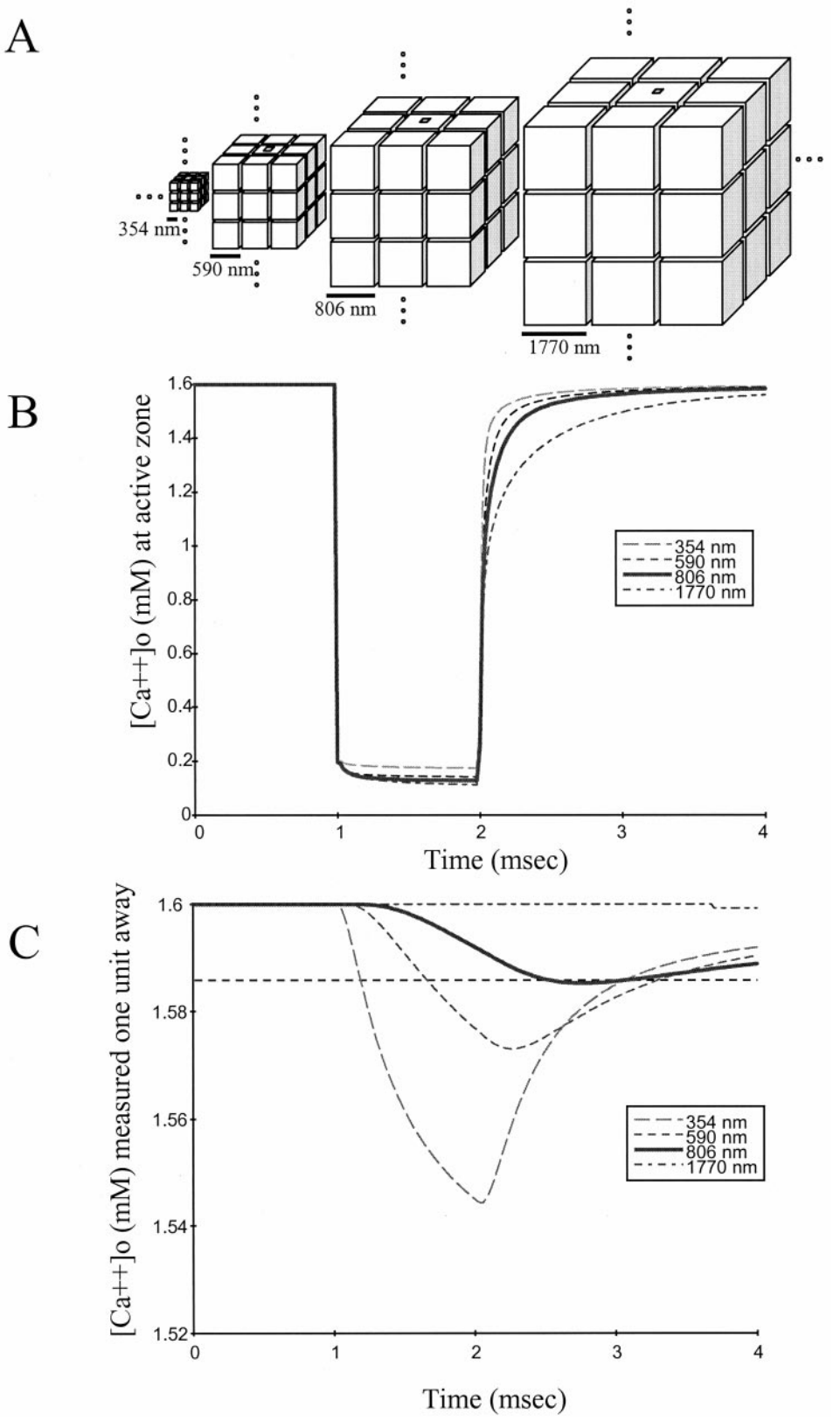

FIGURE 7 (*A*) To examine the effects of changing the size of intracellular elements, the model intracellular units (IUs) are scaled from their default side length of 806 nm. In the following studies, the consuming active zone (represented as the *small shaded square*) always remains the same size: 115 × 115 nm. In all cases, the cleft size between the IUs is maintained at 20 nm. As always, the diagrammed groups of IUs in this figure are packed within larger volumes (9 × 9) of IUs. (*B*) The calcium available to the active zone is approximately independent of active zone size. $D = 300$ $\mu m^2/s$. (*C*) Smaller terminals thwart autonomy. As IUs grow smaller, their influence reaches more units, even though the absolute spatial extent of their signal has decreased. At the realistic terminal size (806 nm per side), the signal measured one unit away from the consumption event is no bigger than the first standard deviation of the expected noise (1.585 mM, *dashed line*; see text). However, for the smallest IU, the signal measured one unit away cannot be interpreted as an expected density fluctuation. Thus only the 806 nm (or bigger) units can have autonomy; i.e., a single consumption event does not interfere with a neighbor's available calcium beyond the expected level of noise.

mately second power at the squid giant synapse (Katz and Miledi, 1970), parallel fiber synapses in the cerebellum (Mintz et al., 1995), and CA3-CA1 fibers in the hippocampus (Qian et al., 1997); at the neuromuscular junction, the relationship is approximately fourth power (Dodge and Rahamimoff, 1967). The calcium signal generated by a single consumptive zone recovers very quickly (usually within 1–2 ms; Figs. 4 and 7), meaning a presynaptic terminal is

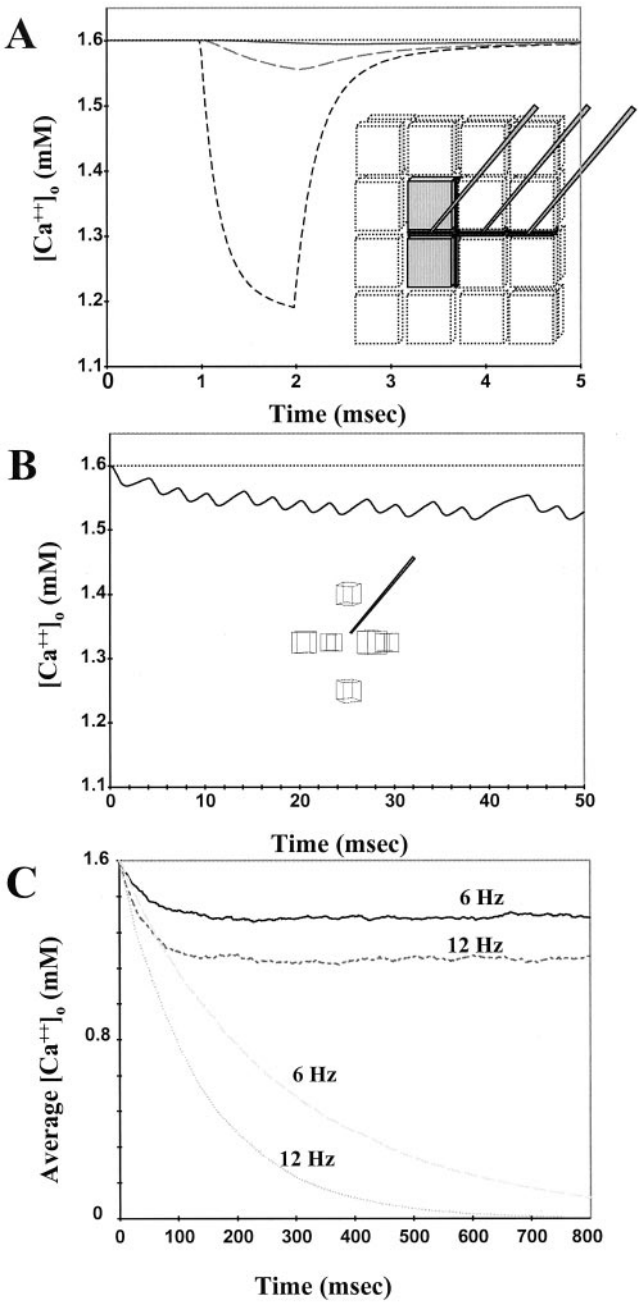

FIGURE 8 Propagation of the calcium fluctuation. (*A*) Available $[Ca^{2+}]_o$ is measured in an active cleft (consumption zone = 806 × 806 nm) and two neighboring clefts in response to calcium consumption for 1 ms. *Lower dashed line*, $[Ca^{2+}]_o$ in active cleft; *middle dashed line*, $[Ca^{2+}]_o$ in first neighboring cleft; *top solid line*, $[Ca^{2+}]_o$ two clefts away, at a distance of 1.6 μm. (*B*) Measurement taken in a cleft in the middle of six simultaneously active units, all at a distance of 1.6 μm (i.e., two clefts away), and all of which are activated synchronously by a real series of spike arrival times from a monkey parvocellular neuron. $D = 300\ \mu m^2/s$. (*C*) The effects of random background activity. All of the units in a 30 × 30 × 30 volume are activated with independent Poisson rates. The mean activity rates shown here are 6 or 12 Hz. In the absence of extrusion mechanisms, all of the calcium in the volume is consumed within 500 ms (*bottom traces*). With rapid first-order extrusion (here half-life = 35 ms), the average $[Ca^{2+}]_o$ (averaged over all clefts) quickly reaches a steady state.

unlikely to interfere with its own transmitter release unless two spikes arrive within about a 1–2-ms window of each other. However, external calcium dynamics might be expected to modulate neighboring terminals within small time windows. More generally, the amount of activity in a region will regulate the average background levels of calcium. Although an individual calcium signal does not travel far from its site of inception, the very large imbalance between the time scales of influx and extrusion (two orders of magnitude) means that quickly heightening activity in a region can lower the available calcium. This would be especially true in situations where the continuity of the ECS is limited, e.g., where consuming elements are sheathed by glial cells. In this way, consumption by a set of elements can lower the available calcium to other elements, implementing a form of presynaptic inhibition.

An important form of presynaptic inhibition may also be implemented by back-propagating action potentials in dendrites (Egelman and Montague, 1998). Because external calcium in the cleft between the terminal and the dendrite is shared, calcium consumption by a dendrite during a back-propagating action potential (Stuart and Sakmann, 1994; Magee and Johnston, 1995; Yuste and Tank, 1996) can temporarily reduce the amount of calcium available to the terminal. Such calcium decrements may translate into diminished release probabilities—or even a complete veto of release—at the overlying terminals. In other words, a postsynaptic neuron may be able to employ back-propagating action potentials to modulate the neurotransmitter release patterns of afferent terminals. Thus, unlike classical neurotransmission, an external calcium signal may be bidirectional, transmitting information about postsynaptic activity as effectively as presynaptic activity. These issues are explored in Egelman and Montague (1998).

Calcium may delimit how spike patterns translate into patterns of neurotransmitter release

The translation of a one-dimensional "spike code" into a spatiotemporal "neurotransmitter release code" will depend on 1) the neuron's exact spike timing and 2) the three-dimensional distribution of boutons in the tissue. For illustration, consider the close apposition of several boutons from different axons. If spikes along the different axons arrive far out of register with each other, the average Ca^{2+} influx into each terminal may be unaffected. However, in the case of synchronized activity, the average Ca^{2+} influx to each given bouton may be reduced sufficiently to change the pattern of release. Over the entire axonal arbor, a given action potential may lead to release in different subsets of the terminals, depending in part on the local calcium concentration in which each terminal finds itself. The temporal code seen by any postsynaptic element monitoring neurotransmitter release will be a subset of the spike code generated at the axon hillock.

Time scales

Brain function involves a range of temporal and spatial scales. For example, fast neurotransmission, slower neuromodulation, and even slower gene regulation are thought to play a number of important roles. In the same way, transient Ca^{2+} fluctuations may influence rapid signal transfer, whereas slower modulation of background calcium levels could influence attentional states, learning, and reorganization of tissue.

We briefly discuss four mechanisms that give rise to different time scales: 1) different kinetics of Ca^{2+}-fluxing channels, 2) different Ca^{2+}-reading mechanisms, 3) different cell types, and 4) different cellular geometries.

Channels

Thus far we have limited our discussion to generalized voltage-gated conductances. However, the release of neurotransmitter (NT) may gate ligand-sensitive Ca^{2+}-fluxing channels, causing the consumption of thousands more ions (Gasic and Heinemann, 1992). NMDA, ATP, and nicotinic Ach receptor channels show a fractional Ca^{2+} current of 12%, 6.7%, and 4% Ca^{2+}, respectively (Rogers and Dani, 1995); in addition, certain AMPA receptors flux Ca^{2+} (Burnashev et al., 1992; Meucci et al., 1996). The different kinetics of the above channels can lead to different calcium contexts for surrounding cells. For example, NMDA receptors activated by the coincidence of glutamate and depolarization cause Ca^{2+} consumption for many tens of milliseconds (analyzed in Vassilev et al., 1997).

Ca^{2+}-reading mechanisms

Aside from "reading" $[Ca^{2+}]_o$ via influx, a cell might also detect external levels directly. One example is the recently cloned Ca^{2+}-sensing receptor (CaR), a transmembrane G-coupled protein whose activation has a steep sigmoidal dependence on $[Ca^{2+}]_o$ (Brown, 1991; Brown et al., 1993; Ruat et al., 1995). In parathyroid cells, a 2–3% change in $[Ca^{2+}]_o$ can activate the CaR, because the middle of the sigmoid is positioned at the physiological range of concentrations (Brown et al., 1993). The fact that the CaR is expressed in the mammalian brain (Brown et al., 1995) suggests that the alteration of calcium levels in a cleft can be directly sensed. This metabotropic reaction to changes in external calcium will operate on slower time scales than the influx and binding of calcium to enzymes. As a second example, rapid functional effects are sometimes expressed in channel dynamics: in squid giant neurons, external calcium levels quickly modulate both the gating and selectivity of K^+ channels (Armstrong and Lopez-Barneo, 1987).

Cell types

Calcium-permeable channels cover dendrites, axonal terminals, and somas of neurons. However, neurons are 10 times less plentiful than glial cells in the brain. Although a supporting or trophic role has traditionally been favored for glial cells, there are mounting data on glial cell consumption of external calcium. Glial cells express voltage-gated calcium channels (Verkhratsky and Kettenmann, 1996) and ligand-gated Ca^{2+} channels (Burnashev et al., 1992), and there is even the suggestion that the Na^+/Ca^{2+} transporter can reverse under conditions of lowered $[Na^+]_o$, taking Ca^{2+} in from the ECS (Brown et al., 1995; Chebabo et al., 1995; Verkhratsky and Kettenmann, 1996).

Geometry

The ECS may not be continuous. In a closed volume (such as a glomerulus sheathed by glial cells), it is possible that a relatively fixed amount of external calcium is shared by the terminals and dendrites of that volume. In this way, recovery time would be much slower than in the examples presented here, and recovery would depend in large part on extrusion rates. This notion is consistent with a mathematical analysis of astrocytic partial sheathing of a synapse (Smith, 1992).

The role of other ionic species

Calcium is an attractive extracellular species because of its known importance to so many signaling functions (Bootman and Berridge, 1995). However, the implications of our results here may apply to other extracellular ion species as well. Measurements of $[Ca^{2+}]_o$ are often made in conjunction with $[K^+]_o$, which is also low relative to $[Na^+]_o$ and $[Cl^-]_o$. Under normal conditions, $[K^+]_o$ fluctuates from 3 mM up to ~7 mM in the mammalian cortex (Lebovitz, 1996; Sykova, 1997). This could have a substantial effect on neural function, most obviously by its effect on resting membrane potentials. Moreover, concomitant decreases in $[Na^+]_o$ during activity can secondarily affect $[Ca^{2+}]_o$: it has been shown in hippocampal slices that decreasing $[Na^+]_o$ from 154 to 114 mM significantly reduces $[Ca^{2+}]_o$, most likely through an osmolality-sensing mechanism involving the Na^+/Ca^{2+} exchanger (Brown et al., 1995; Chebabo et al., 1995).

CONCLUSION

Using a model of the extracellular space, we have explored external calcium fluctuations over a range of parameters, varying the local diffusion coefficient, the rate of consumption, the clustering of the channels, the cleft size, and the geometry of the intracellular elements. We define and explore reasonable ranges for the parameters, including the diffusion coefficient, cleft width, size of the active zone, volume of synaptic elements, linear extent of calcium sinks, and total calcium influx. Under most ranges of these parameters, we have shown that substantial fluctuations are expected to occur during normal activity. The results pre-

sented here indicate that external calcium dynamics, of necessity, will be involved in an understanding of neural encoding and processing of information.

We acknowledge Saurabh Sinha, Michael Wiest, Jing Qian, Richard King, and Sam McClure for helpful comments and criticisms. We also thank Dr. John Maunsell for generously providing electrophysiological data from dorsal lateral geniculate neurons.

This work was supported by the Center for Theoretical Neuroscience at Baylor College of Medicine and National Institutes of Mental Health grant RO1 MH52797 (PRM).

REFERENCES

Armstrong, C. M., and J. Lopez-Barneo. 1987. External calcium ions are required for potassium channel gating in squid neurons. *Science.* 236: 712–714.

Atluri, P. P., and W. G. Regehr. 1996. Determinants of the time course of facilitation at the granule cell to Purkinje cell synapse. *J. Neurosci.* 16:5661–5671.

Benninger, C., J. Kadis, and D. Prince. 1980. Extracellular calcium and potassium changes in hippocampal slices. *Brain Res.* 187:165–182.

Bootman, M., and M. Berridge. 1995. The elemental principles of calcium signaling. *Cell.* 83:675–678.

Brown, E. M. 1991. Extracellular Ca^{2+} sensing, regulation of parathyroid cell function, and role of Ca^{2+} and other ions as extracellular (first) messengers. *Physiol. Rev.* 71:371–411.

Brown, E., G. Gamba, D. Riccardi, M. Lombardi, R. Butters, O. Kifor, A. Sun, M. Hediger, J. Lytton, and S. Herbert. 1993. Cloning and characterization of an extracellular Ca^{2+}-sensing receptor from bovine parathyroid. *Nature.* 71:575–580.

Brown, E. M., P. M. Vassilev, and S. C. Herbert. 1995. Calcium ions as extracellular messengers. *Cell.* 83:679–682.

Burnashev, N., A. Khodorova, P. Jonas, P. Helm, W. Wisden, H. Monyer, P. Seeburg, and B. Sakmann. 1992. Calcium-permeable AMPA-kainate receptors in fusiform cerebellar glial cells. *Science.* 256:1566–1570.

Chebabo, S., M. Hester, J. Jing, P. Aitken, and G. Somjen. 1995. *J. Physiol.* 487:686–697.

Colman, H., and J. W. Lichtman. 1992. Cartellian competition at the neuromuscular junction. *Trends Neurosci.* 15:197–199.

Dodge, F. A., and R. Rahamimoff. 1967. Co-operative action of calcium ions in transmitter release at the neuromuscular junction. *J. Physiol. (Lond.).* 193:419–432.

Egelman, D. M., and P. R. Montague. 1998. Computational properties of peri-dendritic calcium fluctuations. *J. Neurosci.* 18:8580–8589.

Gasic, G., and S. Heinemann. 1992. Determinants of the calcium permeation of ligand-gated cation channels. *Curr. Opin. Cell Biol.* 4:670–677.

Heinemann, U., J. Stabel, and G. Rausche. 1990. Activity-dependent ionic changes and neuronal plasticity in rat hippocampus. *Prog. Brain Res.* 83:197–214.

Helmchen, F., G. G. Borst, and B. Sakmann. 1997. Calcium dynamics associated with a single action potential in a CNS presynaptic terminal. *Biophys. J.* 72:1458–1471.

Helmchen, F., K. Imoto, and B. Sakmann. 1996. Ca^{2+} buffering and action-potential-evoked Ca^{2+} signalling in dendrites of pyramidal neurons. *Biophys. J.* 70:1069–1081.

Jones, H. C., and R. F. Keep. 1987. The control of potassium concentration in the cerebrospinal fluid and brain interstitial fluid of developing rats. *J. Physiol. (Lond.).* 383:441–453.

Katz, B., and R. Miledi. 1970. Further study of the role of calcium in synaptic transmission. *J. Physiol. (Lond.).* 207:789–801.

Lebovitz, R. 1996. Quantitative examination of dynamic interneuronal coupling via single-spike extracellular potassium ion transients. *J. Theor. Biol.* 180:11–25.

Loewi, O., and E. Navratil. 1926. On the humoral propagation of cardiac nerve action. *In* Cellular Neurophysiology: A Source Book. I. Cooke and M. Lipkin, editors. Holt, Rinehart and Winston, Orlando, FL. 478–485.

Mackensie, P. J., M. Umemiya, and T. H. Murphy. 1996. Ca^{2+} imaging of CNS axons in culture indicates reliable coupling between single action potentials and distal functional release sites. *Neuron.* 16:783–795.

Magee, J., and D. Johnston. 1995. Characterization of single voltage-gated Na^{+} and Ca^{2+} channels in apical dendrites of rat CA1 pyramidal cells. *J. Physiol. (Lond.).* 487.1:67–90.

Meucci, O., A. Fatatis, J. Holzwarth, and R. Miller. 1996. Developmental regulation of the toxin sensitivity of Ca(2+)-permeable AMPA receptors in cortical glia. *J. Neurosci.* 16:519–530.

Mintz, I., B. Sabatini, and W. Regehr. 1995. Calcium control of transmitter release at a central synapse. *Neuron.* 15:675–688.

Montague, P. R. 1996. The resource consumption principle: attention and memory in volumes of neural tissue. *Proc. Natl. Acad. Sci. USA.* 93:3619–3623.

Nicholson, C. 1980. Modulation of extracellular calcium and its functional implications. *Fed. Proc.* 39:1519–1523.

Nicholson, C., and J. M. Phillips. 1981. Ion diffusion modified by tortuosity and volume fraction in the extracellular microenvironment of the rat cerebellum. *J. Physiol. (Lond.).* 321:225–257.

Nicholson, C., G. tenBruggencate, H. Stockle, and R. Steinberg. 1978. Calcium and potassium changes in extracellular microenvironments of cat cerebellar cortex. *J. Neurophysiol.* 41:1026–1039.

Philipson, K., and D. Nicoll. 1993. Molecular and kinetic aspects of sodium-calcium exchange. *Int. Rev. Cytol.* 137C:199–227.

Qian, J., W. F. Colmers, and P. Saggau. 1997. Inhibition of synaptic transmission by neuropeptide Y in rat hippocampal area CA1: modulation of presynaptic calcium entry. *J. Neurosci.* 17:8169–8177.

Regehr, W. G., and D. W. Tank. 1990. Postsynaptic NMDA receptor-mediated calcium accumulation in hippocampal CA1 pyramidal cell dendrites. *Nature.* 345:807–810.

Roberts, W. M., R. A. Jacobs, and A. J. Hudspeth. 1990. Colocalization of ion channels involved in frequency selectivity and synaptic transmission at presynaptic active zones of hair cells. *J. Neurosci.* 10:3664–3684.

Robitaille, R., E. M. Adler, and M. P. Charlton. 1990. Strategic localization of calcium channels at transmitter release sites of frog neuromuscular synapses. *Neuron.* 5:773–779.

Rogers, M., and J. A. Dani. 1995. Comparison of quantitative calcium flux through NMDA, ATP, and ACh receptor channels. *Biophys. J.* 68: 501–506.

Ruat, M., M. E. Molliver, A. M. Snowman, and S. Snyder. 1995. Calcium sensing receptor: molecular cloning in rat and localization to nerve terminals. *Proc. Natl. Acad. Sci. USA.* 92:3161–3165.

Schatzmann, H. 1989. The calcium pump of the surface membrane and of the sarcoplasmic reticulum. *Annu. Rev. Physiol.* 51:473–485.

Sinha, S. R., L. Wu, and P. Saggau. 1997. Presynaptic calcium dynamics and transmitter release evoked by single action potentials at mammalian central synapses. *Biophys. J.* 72:637–651.

Smith, S. J. 1992. Do astrocytes process neural information? *In* Neuronal-Astrocytic Interactions. Implications for Normal and Pathological CNS Function. A. C. H. Yu, L. Hertz, M. D. Norenberg, E. Sykova, and S. G. Waxman, editors. Elsevier Science, New York. 119–136.

Smith, S. J., and G. J. Augustine. 1988. Calcium ions, active zones and neurotransmitter release. *Trends Neurosci.* 11:458–464.

Stuart, G., and B. Sakmann. 1994. Active propagation of somatic action potentials into neocortical pyramidal cells dendrite. *Nature.* 367:69–72.

Sykova, E. 1997. The extracellular space in the CNS: its regulation, volume and geometry in normal and pathological neuronal function. *Neuroscientist.* 3:28–41.

Tank, D. W., W. G. Regehr, and K. R. Delaney. 1995. A quantitative analysis of presynaptic calcium dynamics that contribute to short-term enhancement. *J. Neurosci.* 15:7940–7952.

Vassilev, P. M., J. Mitchel, M. Vassilev, M. Kanazirska, and E. M. Brown. 1997. Assessment of frequency-dependent alterations in the level of extracellular Ca^{2+} in the synaptic cleft. *Biophys. J.* 72:2103–2116.

Verkhratsky, A., and H. Kettenmann. 1996. Calcium signalling in glial cells. *Trends Neurosci.* 19:346–352.

Yuste, R., and D. Tank. 1996. Dendritic integration in mammalian neurons, a century after Cajal. *Neuron.* 16:701–716.